



# Low-level NO gas sensing properties of $\text{Zn}_{1-x}\text{Sn}_x\text{O}$ nanostructure sensors under UV light irradiation at room temperature

IRMAK KARADUMAN ER<sup>1,\*</sup>, ALI ORKUN ÇAĞIRTEKİN<sup>1</sup>, TUĞBA ÇORLU<sup>1</sup>,  
MEMET ALI YILDIRIM<sup>2</sup>, AYTUNÇ ATEŞ<sup>3</sup> and SELİM ACAR<sup>1</sup>

<sup>1</sup>Department of Physics, Science Faculty, Gazi University, Ankara 06500, Turkey

<sup>2</sup>Department of Electric and Electronics Engineering, Engineering Faculty, Erzincan University, Erzincan 25050, Turkey

<sup>3</sup>Department of Material Engineering, Engineering and Natural Sciences Faculty, Yıldırım Beyazıt University, Ankara 06500, Turkey

\*Author for correspondence (karaduman.irmak@gmail.com)

MS received 28 August 2017; accepted 19 July 2018; published online 2 February 2019

**Abstract.**  $\text{Zn}_{1-x}\text{Sn}_x\text{O}$  ( $x = 0, 0.05, 0.10, 0.15, 0.20$ ) nanostructures have been grown through the successive ionic layer adsorption and reaction method. The structural, morphological and compositional properties of the nanostructures have been characterized through X-ray diffraction, scanning electron microscope and energy dispersive X-ray analysis, respectively. The NO gas sensing properties of sensors to 20 ppb have been systematically investigated in the dark and under UV light irradiation. A  $\text{Zn}_{0.90}\text{Sn}_{0.10}\text{O}$  sensor has exhibited the highest response for 20 ppb NO gas compared with other sensors. The sensor response has increased from 1.9 to 43% depending on the UV light irradiation for the  $\text{Zn}_{0.90}\text{Sn}_{0.10}\text{O}$  sensor.  $\text{Zn}_{0.90}\text{Sn}_{0.10}\text{O}$  nanostructure can be used as a suitable gas sensor material for detection of low concentration levels of NO gas.

**Keywords.** Gas sensor; UV light irradiation; Sn-doped ZnO nanostructures.

## 1. Introduction

It is well-known that the working principle of a metal oxide gas sensor is based on the surface chemical reaction which perturbs the free carrier density within the metal oxide. It is the variation of the electrical properties of the sensor to gas that can be used for detecting the change in the surrounding atmosphere [1]. Semiconducting metal oxide (MOS) gas sensors have attracted considerable attention because of their many advantages over traditional chemical analysis methods. These advantages include fast response, high sensitivity, small dimensions, ease of use, portability, simple design and fabrication, real-time detection, low detection limits, low cost and low power consumption [2].

Metal oxide gas sensors are generally operated above 100°C to overcome the energy limit of chemisorption for reaching high sensitivity [1,2]. The elevated temperature provides energy for the chemisorption and reaction of gaseous species on the surface. Heating accounts for approximately all the energy of these sensors. Thus, energy consumption is a challenge in the development of portable products. Furthermore, high temperature may ignite flammable or explosive gases. Several approaches have been proposed to improve the sensor response and reduce the sensor operating temperature [3]. One of the effective approaches is to expose the sensor to UV light irradiation. UV light irradiation enhances the carrier concentration which affects the gas

sensing capability and causes high responses at room temperature [4,5].

In this study, we have focused on increasing the gas sensing performance of  $\text{Zn}_{1-x}\text{Sn}_x\text{O}$  nanostructures. UV light irradiation has affected the gas sensing properties of the sensors and has caused to give high responses of the sensors for 20 ppb NO gas at room temperature.

## 2. Experimental

$\text{Zn}_{1-x}\text{Sn}_x\text{O}$  ( $x = 0, 0.05, 0.10, 0.15, 0.20$ ) nanostructures have been grown through the successive ionic layer adsorption and reaction (SILAR) method on the glass substrates ( $8 \times 25 \text{ mm}^2$ ) on which the interdigitated Au electrodes (Au-IDEs) have been evaporated to a side of substrate. The glass substrates have been ultrasonically cleaned for 10 min, first in acetone and then in an ethanol:water (1:1) solution. The cleaned glass substrates have been then dried under nitrogen gas. After the drying process has been completed, the Au-IDEs have been evaporated to a side of the glass substrates through an e-beam evaporation system. The width and area of the Au-IDEs are approximately 0.7 mm and  $14 \times 7 \text{ mm}^2$ , respectively.

To grow  $\text{Zn}_{1-x}\text{Sn}_x\text{O}$  nanostructures, aqueous zinc-ammonia complex ions ( $[\text{Zn}(\text{NH}_3)_4]^{2+}$ ) and aqueous tin-ammonia complex ions ( $[\text{Sn}(\text{NH}_3)_4]^{4+}$ ) have been chosen

as the cation precursors, in which trace metal basis of  $\text{ZnCl}_2$  (99.9%, Sigma-Aldrich) of 0.1 M,  $\text{SnCl}_4$  (99.9%, Sigma-Aldrich) of 0.1 M as sources for Zn, Sn and aqueous ammonia solution ( $\text{NH}_3$ -28%, Sigma-Aldrich) have been used. Deionized water has been used as a solvent. The obtained  $[\text{Zn}(\text{NH}_3)_4]^{2+}$  and  $[\text{Sn}(\text{NH}_3)_4]^{4+}$  complexes have been mixed in appropriate proportions according to the composition for  $\text{ZnO}$ ,  $\text{Zn}_{0.95}\text{Sn}_{0.05}\text{O}$ ,  $\text{Zn}_{0.90}\text{Sn}_{0.10}\text{O}$ ,  $\text{Zn}_{0.85}\text{Sn}_{0.15}\text{O}$  and  $\text{Zn}_{0.80}\text{Sn}_{0.20}\text{O}$  nanostructures. All the growth process parameters of  $\text{Zn}_{1-x}\text{Sn}_x\text{O}$  nanostructures through the SILAR method have been elaborately described in the previous studies [6–8].  $\text{Zn}_{1-x}\text{Sn}_x\text{O}$  nanostructures have been grown by repeating 40 SILAR cycles. The nanostructures have been annealed under a nitrogen atmosphere (300°C, 15 min) and characteristic parameters of the nanostructures have been investigated.

For structural, morphological and compositional studies, a Panalytical Empyrean X-ray Diffractometer (using  $\text{Cu K}\alpha$   $\lambda = 1.5405 \text{ \AA}$  radiation), an FEI Quanta FEG 450 model SEM with energy dispersive X-ray analysis (EDAX) attachment have been used. The gas sensing performance of the sensors has been tested with a gas sensing measurement system. The working principle of the gas sensing measurement system has been given in the previous work [8,9]. The gas sensing measurements have been carried out for NO gas at different concentrations and operating temperatures by monitoring the resistance changes. Dry air has been used as the carrier gas, which is 99.9% purity (dry air is the ‘blank’ gas used to purge the sensor). The flow rate of the dry air undergoing testing has been fixed at  $500 \text{ cm}^3 \text{ min}^{-1}$  during the measurements. Air flow rate, under the same conditions in order to observe the behaviour of different concentrations must be kept always constant. To ensure stable zero-level resistance in ambient air prior to exposure to gas the stabilization of the nanostructure resistance is important because it ensures stable zero level for gas sensing applications. For the corresponding operating temperature of the gas chamber, it is the prime requisite to stabilize the resistance in air atmosphere before ejecting the gas into the chamber. It indicates the resistance of nanostructure in air. The NO concentration and dry airflow rates have been controlled by computer controlled mass flow controllers (MKS series). The LakeShore 325 temperature controller with platinum resistance temperature detectors has been used to maintain a constant temperature. The sensor resistance has been continuously monitored with a computer controlled system using a Keithley 2400 source meter. The data have been collected in real-time using a computer with corresponding data acquisition hardware and software. Relative humidity has been kept constant (about 25%) for all measurements, monitored by the Honeywell HIH-4000 humidity sensor. The measurements have been carried out under UV light irradiation (UVGL-58 handheld lamp) with 365 nm wavelength and  $1200 \mu\text{W cm}^{-2}$  irradiation intensity. Before the measurements, sensors under test have been fixed into the chamber and the sensors have been kept constant at 130°C for

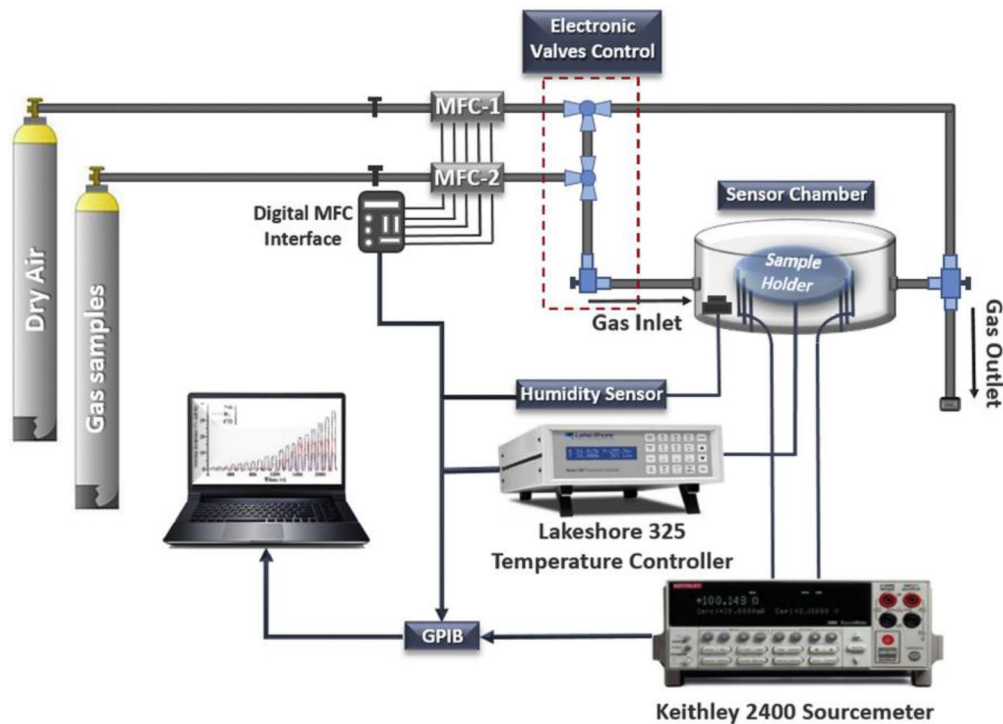
20 min to enhance the adhesion. Figure 1 shows the schematic diagram of the computer-controlled gas sensing measurement system.

### 3. Results and discussion

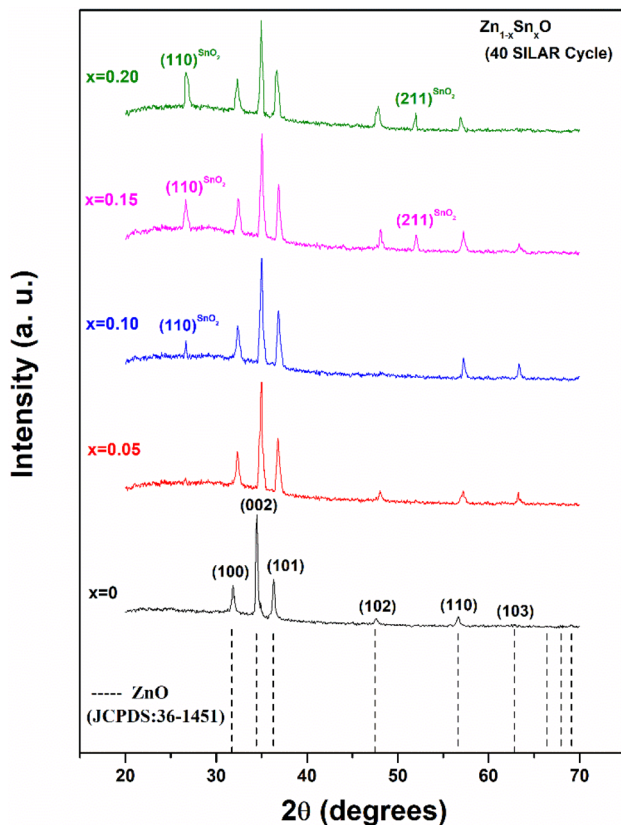
Figure 2 shows the X-ray diffraction (XRD) patterns of  $\text{Zn}_{1-x}\text{Sn}_x\text{O}$  nanostructures. As seen in figure 2, a  $\text{ZnO}$  nanostructure ( $x = 0$ ) has a hexagonal wurtzite phase (JCPDS card no. 36-1451) [7]. The intensities and full width at half maximum (FWHM) values of the characteristic peaks of  $\text{ZnO}$  change and some peaks disappear with increasing Sn concentration ( $x$ ), whereas the characteristic peaks belonging to the tetragonal phase (JCPDS card no. 41-1445) of the  $\text{SnO}_2$  nanostructure begin to appear and the intensity of the peaks increases with increasing Sn concentration ( $x$ ). It has been observed that the dominant crystal phase in all the XRD patterns of the nanostructures is the hexagonal wurtzite phase of  $\text{ZnO}$ . Also, the peak positions with Sn concentration ( $x$ ) have been determined to shift with slightly larger diffraction angles. It has been related to the unit cell size changes in nanostructures with the substitution of  $\text{Sn}^{4+}$  for  $\text{Zn}^{2+}$ , because the ionic radii of  $\text{Zn}^{2+}$  (0.74 Å) and  $\text{Sn}^{4+}$  (0.69 Å) are different [10–12].

Figure 3 shows the scanning electron microscopy (SEM) images and EDAX analysis of  $\text{Zn}_{1-x}\text{Sn}_x\text{O}$  nanostructures. As seen in figure 3, all the nanostructures have a compact, dense surface morphology and cover the substrates very well.  $\text{ZnO}$  has nanorod structure and localized clusters on the surface morphology.  $\text{Zn}_{0.95}\text{Sn}_{0.05}\text{O}$  has porous sphere and localized flower-like structures.  $\text{Zn}_{0.90}\text{Sn}_{0.10}\text{O}$  has uniform and well-grown porous sphere structure. The SEM image of  $\text{Zn}_{0.85}\text{Sn}_{0.15}\text{O}$  has been composed of a large number of uniform nanoballs. It has been clearly seen that the uniformity and smoothness of  $\text{Zn}_{0.80}\text{Sn}_{0.20}\text{O}$  have decreased compared with the other nanostructures. Consequently, the diversity in surface morphology of Sn-doped  $\text{ZnO}$  materials is a key factor in the sensing performance for the gas sensors [13]. EDAX analysis shows the presence of Zn, Sn and O elements in the nanostructures. The atomic percent values of these elements in the nanostructures have been given in the inset of EDAX. The presence of Si and Ca elements may originate from the substrate.

Figure 4a shows the  $I$ – $V$  characteristics of the  $\text{Zn}_{1-x}\text{Sn}_x\text{O}$  nanostructure-based sensors at room temperature. The changes in the slope of the curves are due to the change in the sensor resistance which is associated with the doping concentrations. The operating temperature is an important factor that can essentially influence the catalytic properties of the sensing material, especially in the case of noble metal-modified semiconducting oxides [8–14]. It affects the electron mobility and the electrical conductivity of the metal oxide material. The operating temperature influences the chemical dynamics at the gas–solid interface and thus it affects the important sensing properties such as response, selectivity, stability, response



**Figure 1.** The schematic diagram of the gas sensing measurement system.

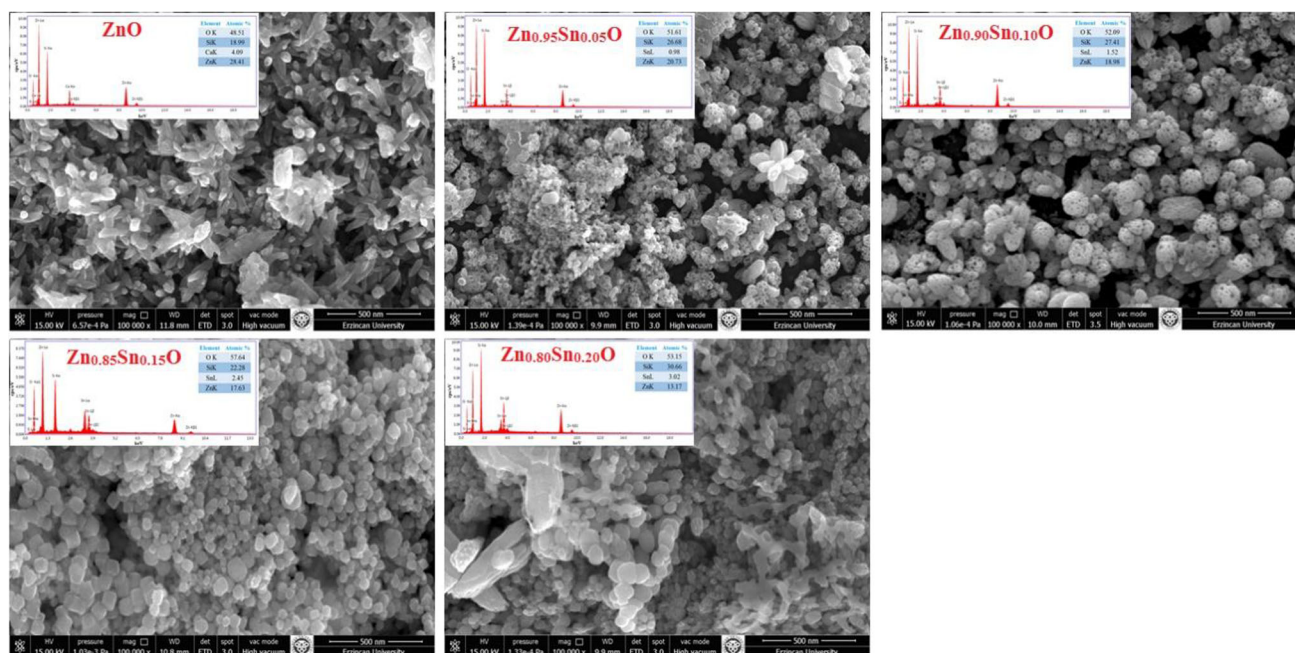


**Figure 2.** The XRD patterns of  $\text{Zn}_{1-x}\text{Sn}_x\text{O}$  nanostructures.

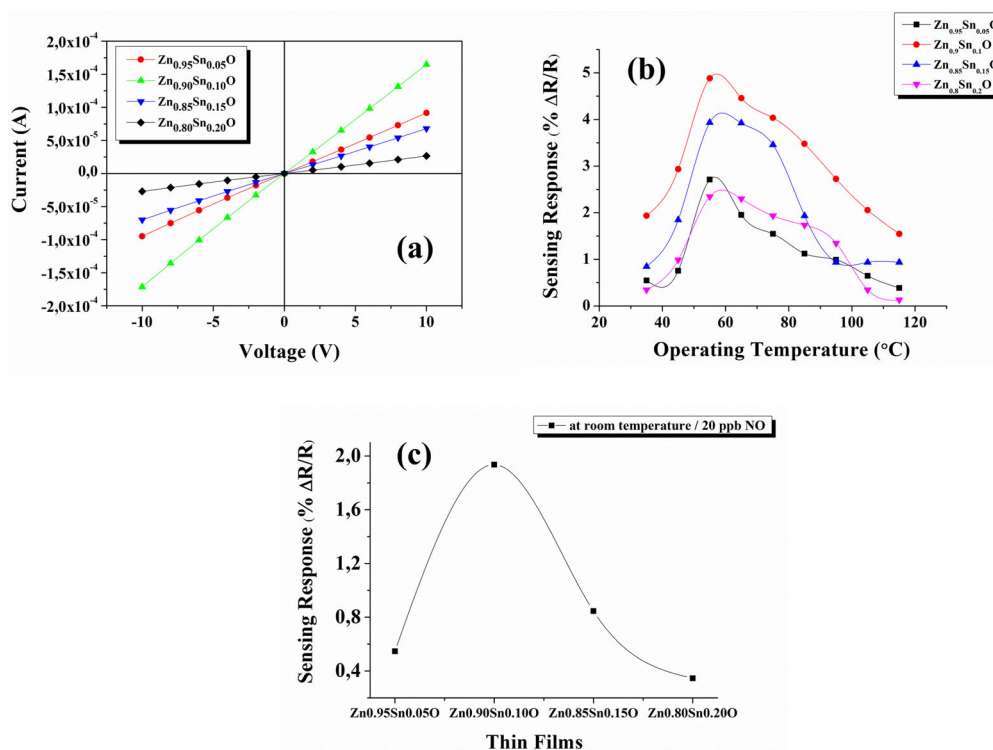
and recovery times [8–14]. There usually exists a temperature region, in which the sensor reveals the highest sensitivity. However, the high temperature causes the deterioration of the sensing surface due to high-power consumption. Gas sensing measurements based on working temperature have been carried out to find the optimal working temperature. The responses of the sensors for 20 ppb NO gas at different temperatures are shown in figure 4b. The operating temperature plays a crucial role in gas adsorption/desorption as well as the chemical reaction between surface adsorbed oxygen and NO molecules. Sensing material exhibits a maximum response towards a target gas at an optimal temperature [8–14]. The operating temperature has been found to be 55°C for all the nanostructure-based sensors. The responses of  $\text{Zn}_{0.95}\text{Sn}_{0.05}\text{O}$ ,  $\text{Zn}_{0.90}\text{Sn}_{0.10}\text{O}$ ,  $\text{Zn}_{0.85}\text{Sn}_{0.15}\text{O}$  and  $\text{Zn}_{0.80}\text{Sn}_{0.20}\text{O}$  sensors for 20 ppb NO gas at 55°C have been calculated to be 2.7, 5, 3.9 and 2.3%, respectively. Figure 4c shows the responses of sensors for 20 ppb NO gas concentration at room temperature. The responses of  $\text{Zn}_{0.95}\text{Sn}_{0.05}\text{O}$ ,  $\text{Zn}_{0.90}\text{Sn}_{0.10}\text{O}$ ,  $\text{Zn}_{0.85}\text{Sn}_{0.15}\text{O}$  and  $\text{Zn}_{0.80}\text{Sn}_{0.20}\text{O}$  sensors for 20 ppb NO gas at room temperature have been calculated to be 0.5, 1.9, 0.85 and 0.34%, respectively. There is no response for 20 ppb NO gas obtained for pure ZnO nanostructure.

Figure 5 shows selectivity measurements at 55°C operating temperature for the sensors. Selectivity of the sensor also plays a vital role in evaluating the efficiency of the gas sensor. The selectivity of the sensor to gas molecules is greatly affected by the chemical composition of sensor





**Figure 3.** The SEM images and EDAX analysis of  $\text{Zn}_{1-x}\text{Sn}_x\text{O}$  nanostructures.



**Figure 4.** (a) The  $I$ - $V$  characteristics of  $\text{Zn}_{1-x}\text{Sn}_x\text{O}$  sensors at room temperature, (b) the responses of 20 ppb NO for  $\text{Zn}_{1-x}\text{Sn}_x\text{O}$  sensors as a function of operating temperature and (c) the responses of 20 ppb NO for  $\text{Zn}_{1-x}\text{Sn}_x\text{O}$  sensors at room temperature.

materials as well as by the operating temperature of the sensor. This allows us to propose the different chemical and physical nature of the sensor response in the case of each target gas

which requires particular consideration. The sensor responses obtained towards  $\text{CO}_2$ ,  $\text{H}_2$ , ethanol and acetone gases are negligible values due to the low-operating temperature.

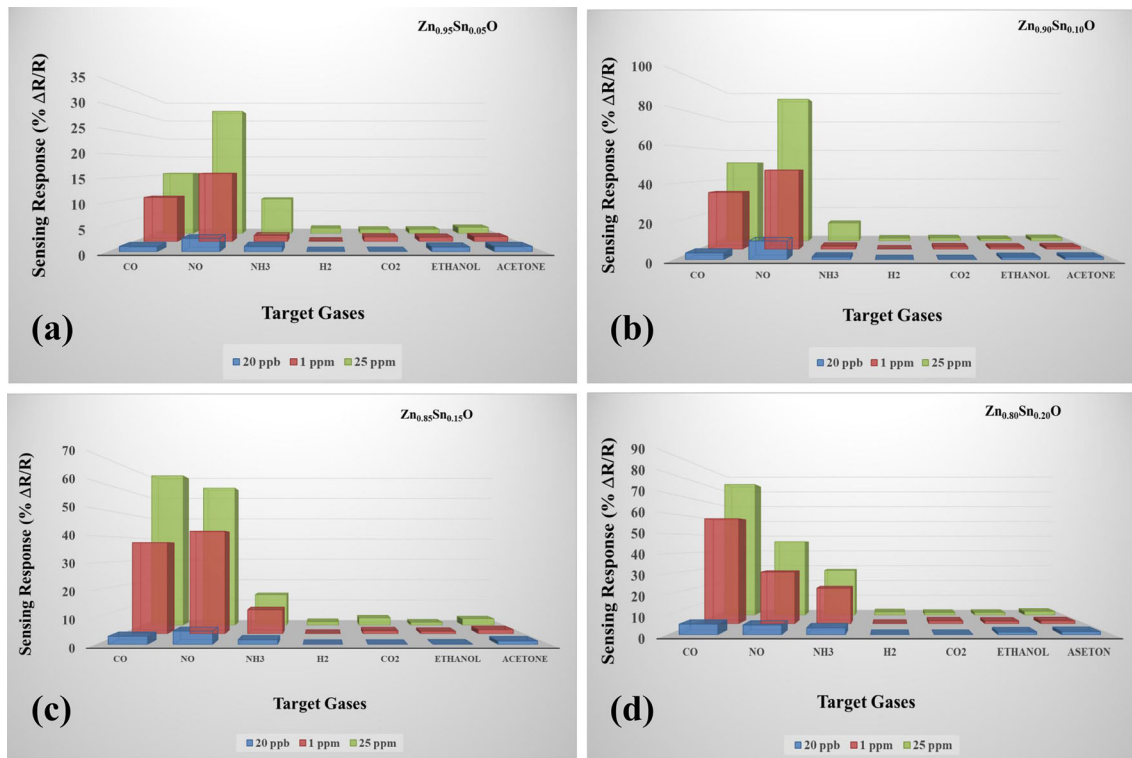


**Figure 5.** The selectivity of  $\text{Zn}_{1-x}\text{Sn}_x\text{O}$  sensors.

It is well-known that the working principle of the metal oxide gas sensor is based on the surface chemical reaction, which perturbs the free carrier density within the metal oxide. It is the variation of the electrical properties of the sensor with gas that can be used for detecting the change in the surrounding atmosphere [15]. Metal oxide gas sensors are generally operated above  $100^\circ\text{C}$  to overcome the energy limit of chemisorption for reaching high sensitivity. Exposing the sensors to UV light irradiation leads to a strong increase in the sensor response at temperatures as low as room temperature. For this purpose, the gas sensing measurements have been repeated under UV light irradiation. The relative humidity has been kept constant for all measurements (25%). At low humidity, the conduction process is dominated mainly by electrical conduction whereas, at high humidity, proton conduction plays a significant role in the increase of the total conductivity and it is dominated by the decomposition and the polarization of the absorbed water. In addition, the adsorbed water captures the electrons and the holes generated by UV light irradiation at higher humidity [15]. The responses of the sensors for a constant 20-ppb NO gas concentration have been investigated under UV light irradiation (figure 6a). It has been clearly seen that UV light irradiation has significantly increased the sensor response at room temperature. The  $\text{Zn}_{0.90}\text{Sn}_{0.10}\text{O}$  sensor has exhibited the highest response for 20-ppb NO gas. The sensor response has been calculated

as 1.9% without UV light irradiation, whereas it has been calculated as 43% under UV light irradiation for a  $\text{Zn}_{0.90}\text{Sn}_{0.10}\text{O}$  nanostructure-based sensor. Figure 6b shows the responses of nanostructure sensors as a function of doping concentration (Sn). Moreover, it has been found that the sensor response has increased up to 10% Sn concentration and has decreased after 10% Sn concentration. Figure 6c shows the dynamic gas sensing measurements of the  $\text{Zn}_{0.90}\text{Sn}_{0.10}\text{O}$  sensor. The sensor response has been calculated as almost 80% for 100 ppb NO gas. Figure 6d shows the sensor response with and without 20 ppb NO gas for the  $\text{Zn}_{0.90}\text{Sn}_{0.10}\text{O}$  sensor under UV light irradiation. The response and recovery times have been calculated at 30 and  $55^\circ\text{C}$  operating temperatures and under UV light irradiation at  $30^\circ\text{C}$  as given in table 1. It has been seen that the response and recovery times has varied depending on the doping concentration and the operating temperature. The  $\text{Zn}_{0.90}\text{Sn}_{0.10}\text{O}$  nanostructure-based sensor has the shortest response and recovery times for NO gas. Moreover, it has been found that measurements taken under UV light irradiation have the faster response and recovery times at  $30^\circ\text{C}$  operating temperature.

The sensing mechanism for n-type ZnO based on the modulation of the depletion layer by oxygen absorption can be understood. Electron-hole pairs are created, if photon energy is higher than the bandgap energy of ZnO under UV light irradiation [16]. The photogenerated carriers lead to

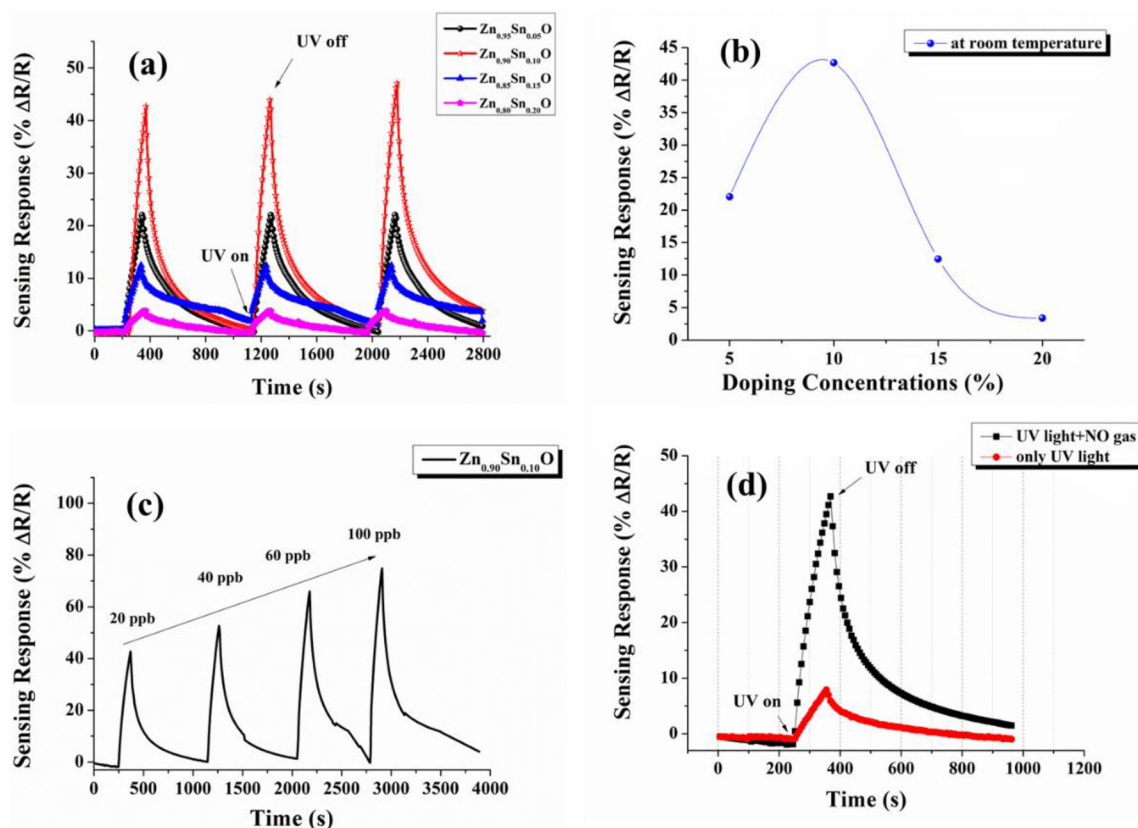
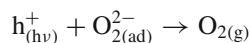


**Figure 6.** (a) The responses of all the Zn<sub>1-x</sub>Sn<sub>x</sub>O sensors for 20 ppb NO gas at room temperature for three cycles, (b) for different doping concentration, (c) the dynamic gas sensing measurements of Zn<sub>0.90</sub>Sn<sub>0.10</sub>O sensor from 20 to 100 ppb and (d) the response with and without 20 ppb NO gas for the Zn<sub>0.90</sub>Sn<sub>0.10</sub>O sensor under UV light irradiation.

**Table 1.** The comparison of response and recovery times.

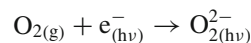
	30°C		55°C		UV light (30°C)	
	Response time (s)	Recovery time (s)	Response time (s)	Recovery time (s)	Response time (s)	Recovery time (s)
20 ppb						
Zn <sub>0.95</sub> Sn <sub>0.05</sub> O	18	20	6	15	6	14
Zn <sub>0.90</sub> Sn <sub>0.10</sub> O	16	29	5	13	5	13
Zn <sub>0.85</sub> Sn <sub>0.15</sub> O	20	32	8	15	6	18
Zn <sub>0.80</sub> Sn <sub>0.20</sub> O	21	35	9	16	11	22

more electrons available to respond to the surrounding O<sub>2</sub> environment change. The photogenerated holes migrate to the surface along the electric field induced by the band bending and discharge chemisorbed oxygen ions following the reaction [17]:



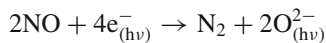
At the same time, oxygen molecules react with the photogenerated electrons and photo-activated oxygen ions (O<sub>2(hv)</sub><sup>2-</sup>) form on the surface. The process occurs until the

adsorption and desorption processes reach steady state following the reaction [18]:



When the nanostructures are stimulated by UV light irradiation, the absorbed oxygen molecules on the surface of ZnO nanostructures are ionized forming O<sub>2(hv)</sub><sup>2-</sup> by capturing electrons from the ZnO conduction band. Oxygen adsorption and desorption reach an equilibrium state, consequently, the

depletion layer is formed and this process causes a higher resistance. When ZnO nanostructures are exposed to an oxidizing gas such as NO, gas molecules capture the electrons on the sensing surface, as shown in the following reaction [19]:



The NO reacts with the surface-adsorbed active oxygen species and is oxidized in the sensing reaction (the surface is reduced) [18,19]. Thus, the concentration of holes increases, increasing the depletion-layer widths in the adjacent grains and decreasing the conducting-channel widths as a result of this resistance increases. NO can capture more electrons, which is attributed to the conducting channel width, and as a result, UV light irradiation can improve the NO gas sensing performance at room temperature [20].

#### 4. Conclusions

$\text{Zn}_{1-x}\text{Sn}_x\text{O}$  ( $x = 0, 0.05, 0.10, 0.15, 0.20$ ) nanostructures have been grown by a simple and facile SILAR method. The low-level NO gas sensing properties of the  $\text{Zn}_{1-x}\text{Sn}_x\text{O}$  nanostructure sensors have been studied under UV light irradiation. The responses of the sensors have been significantly improved under UV light irradiation. Consequently, present results could provide basic and new information for investigations on alternative gas sensor materials.

#### Acknowledgements

This work was supported by TUBITAK with Project No. 115M658 and Gazi University Scientific Research Fund Project No. 05/2016-21.

#### References

- [1] Geng Q, He Z, Chen X, Dai W and Wang X 2013 *Sens. Actuators B* **188** 293
- [2] Mirzaei A, Park S, Kheel H, Sun G-J, Lee S and Lee C 2016 *Ceram. Int.* **42** 6187
- [3] Panda S K and Jacob C 2009 *Bull. Mater. Sci.* **32** 49
- [4] Cho M and Park I 2016 *J. Sens. Sci. Technol.* **25** 103
- [5] Patil P, Gaikwad G, Patil D R and Naik J 2016 *Bull. Mater. Sci.* **39** 655
- [6] Yıldırım M A, Tuna Yıldırım S and Ateş A 2017 *J. Alloys Compd.* **701** 37
- [7] Yıldırım M A, Akaltun Y and Ateş A 2012 *Solid State Sci.* **14** 1282
- [8] Çorlu T, Karaduman I, Yıldırım M A, Ates A and Acar S 2017 *J. Electron. Mater.* **46** 7
- [9] Karaduman I, Er E, Celikkan H and Acar S 2015 *Sens. Actuators B* **221** 1188
- [10] [https://www.webelements.com/periodicity/ionic\\_radius\\_2\\_tet/](https://www.webelements.com/periodicity/ionic_radius_2_tet/)
- [11] Yoo R, Cho S, Song M J and Lee W 2015 *Sens. Actuators B* **221** 217
- [12] Panda J, Sasmal I and Nath T K 2016 *AIP Adv.* **6** 035118
- [13] Zhang Z, Yi J B, Ding J, Wong L M, Seng H L, Wang S J *et al* 2008 *J. Phys. Chem. C* **112** 9579
- [14] Sharma A, Tomar M and Gupta V 2001 *Sens. Actuators B* **156** 743
- [15] Xie W, Liu B, Xiao S, Li H, Wang Y, Cai D *et al* 2015 *Sens. Actuators B* **215** 125
- [16] Espid E and Taghipour F 2017 *Sens. Actuators B* **241** 828
- [17] Luo L, Sosnowchik B D and Lin L 2010 *Nanotechnology* **21** 495502
- [18] Koo W-T, Choi S-J, Kim N-H, Jang J-S and Kim I-D 2016 *Sens. Actuators B* **223** 301
- [19] Jeong Y-J, Balamurugan C and Lee D-W 2016 *Sens. Actuators B* **229** 288
- [20] Karaduman I, Barin Ö, Yıldız D E and Acar S 2015 *J. Appl. Phys.* **118** 174501